Organic Electronics 13 (2012) 320–328

Contents lists available at SciVerse ScienceDirect

Organic Electronics

journal homepage: www.elsevier.com/locate/orgel

Downscaling of *n*-channel organic field-effect transistors with inkjet-printed electrodes

Xiaoyang Cheng [a,1], Mario Caironi [a,b,*,1], Yong-Young Noh [a,c], Christopher Newman [d], Jianpu Wang [a], Mi Jung Lee [a], Kal Banger [a], Riccardo Di Pietro [a], Antonio Facchetti [d], Henning Sirringhaus [a]

[a] Cavendish Laboratory, University of Cambridge, JJ Thomson Avenue, Cambridge CB3 0HE, United Kingdom
[b] Center for Nano Science and Technology @PoliMi, Istituto Italiano di Tecnologia, Via Pascoli 70/3, 20133 Milano, Italy
[c] Department of Chemical Engineering, Hanbat National University, San 16-1, Duckmyoung-dong Yuseong-gu, Daejeon 305-719, Republic of Korea
[d] Polyera Corporation, 8045 Lamon Avenue, Skokie, IL 60077, USA

ARTICLE INFO

Article history:
Received 29 July 2011
Received in revised form 14 November 2011
Accepted 1 December 2011
Available online 13 December 2011

Keywords:
Organic field-effect transistor
Inkjet printing
Bias stress stability
Contact resistance

ABSTRACT

In this contribution we demonstrate for the first time a downscaled *n*-channel organic field-effect transistors based on *N,N′*-dialkylsubstituted-(1,7&1,6)-dicyanoperylene-3,4:9,10-bis(dicarboximide) with inkjet printed electrodes. First we demonstrate that the use of a high boiling point solvent is critical to achieve extended crystalline domains in spin-coated thin films and thus high electron mobility >0.1 $cm^2 V^{-1} s^{-1}$ in top-gate devices. Then inkjet-printing is employed to realize sub-micrometer scale channels by dewetting of silver nanoparticles off a first patterned gold contact. By employing a 50 nm crosslinked fluoropolymer gate dielectric, ~200 nm long channel transistors can achieve good current saturation when operated <5 V with good bias stress stability.

1. Introduction

The performance of solution-processed organic field-effect transistors (OFETs) has improved through new semiconductors development, control of film morphology, optimization of the device geometry, and reduction of the contact resistance [1–8]. Both *p*-channel and *n*-channel OFETs with charge mobilities above 0.1 $cm^2 V^{-1} s^{-1}$ have been demonstrated, providing a solid basis for the realization of solution-processed OFET-based complementary integrated circuits [2,4,5,8–11]. Meanwhile, viable manufacturing techniques compatible with inexpensive fabrication of circuits on flexible substrates and based on environmentally-acceptable processes have been developed [12–16]. Although some OFETs realized via gravure or inkjet printing have been reported, the poor resolution of standard printing technologies has limited the transistors channel length, which is insufficiently small to provide high switching speeds for many applications such as row addressing in active matrix displays or RFID tags [10,17–20]. A solution to this problem is to adopt high resolution printing technologies allowing downscaling of OFET channel lengths, which also requires correct scaling of the dielectric thickness and efficient charge injection in short channels, where optimization of the contact resistance is crucial [19,21]. Currently *p*-channel semiconductors have been widely designed and synthesized with satisfying hole mobilities and device stability, while in the case of *n*-channel semiconductors, only a few candidates can satisfy industrial requirements, mainly due to inefficient electron injection and trapping issues [8,10]. It is usually more difficult to achieve efficient charge injection in *n*-channel OFETs rather than in *p*-channel ones, given the significant mismatch between the Fermi level of noble metals used as electrodes and the lowest unoccupied

* Corresponding author at: Center for Nano Science and Technology @PoliMi, Istituto Italiano di Tecnologia, Via Pascoli 70/3, 20133 Milano, Italy.
E-mail address: mario.caironi@iit.it (M. Caironi).
[1] These authors equally contributed to this work.

1566-1199/$ - see front matter © 2011 Elsevier B.V. All rights reserved.
doi:10.1016/j.orgel.2011.12.001

molecular orbital (LUMO) of most organic *n*-channel semiconductors. Despite a few exceptions [22,23], this leads to severe contact resistance issues which become even more serious when scaling the transistor channel [24]. Therefore most of the short channel, printed OFETs demonstrated so far are fabricated with *p*-channel semiconductors, whereas much less work has been devoted to printed downscaled *n*-channel transistors [25,26].

Among several promising *n*-channel organic semiconductors, *N,N'*-bis(*n*-alkyl)-(1,7&1,6)-dicyanoperylene-3,4:9,10-bis(dicarboximide) derivatives (PDIR-CN_2) have shown great potential for realization of high mobility *n*-channel OFETs and the fabrication of organic complementary circuits [27]. Several PDIR-CN_2 derivatives exhibit excellent *n*-channel performance and remarkable environmental stability both in the case of vapour deposited and solution deposited semiconducting layers [28–30]. Recently it was shown that based on the soluble core-cyanated perylenediimide, ActivInk N1400, electron mobility >0.1 $cm^2 V^{-1} s^{-1}$ can be obtained in staggered, solution-processed *n*-channel OFETs [31,32]. Here we use N1400 as the base of our study with the aim to realize downscaled, low-voltage *n*-channel FETs, as test-beds for commercially-relevant applications. First we demonstrate that in order to achieve high electron mobility in N1400 based OFETs, the use of a high boiling point solvent is essential. When 1,2-dichlorobenzene (DCB) is used instead of chloroform, a higher degree of crystallinity is achieved, favouring both electron transport and device stability under bias stress condition. Although the contact resistance extrapolated from the top-gate *n*-channel transistor with Au contacts is relatively low, we show that it is not sufficient to achieve good downscaled transistors because of severe contact effects in the short channel devices. This can be strongly improved by adopting silver electrodes, thus allowing to downscale the channel length for this *n*-channel device to a few hundreds of nanometers while preserving correct field-effect behaviour despite some injection limitation. Downscaled printed OFETs were fabricated by inkjet printing silver nanoparticles (AgNPs) for the injecting contact. The lower work-function (W_f) of these contacts with respect to evaporated Ag electrodes is found to be crucial for the correct downscaling. This approach, together with the use of an ultra-thin crosslinked fluoropolymer gate dielectric, allows full current saturation behaviour at operating voltages <5 V.

2. Materials and methods

In this study we realized various FETs with various device configuration: bottom-gate, bottom-contacts (Fig. 1(a)) and top-gate, bottom-contacts (Fig. 1 (b) and (c)) FETs, with photolithographically defined Au contacts (Fig. 1(a) and (b)) or inkjet printed Ag electrodes (Fig. 1(c)). A n^{++} silicon wafer with 300 nm oxide served for bottom-gate structures and corning 1737F glass substrates were used for the top-gate configurations. Gold source-drain contacts were photolithographically defined using a double layer lift-off process. *N*-channel ActivInk N1400 semiconductor (*N,N'*-dialkyl-(1,7&1,6)-dicyano-tetracarboximide, Polyera Corporation) dissolved in different solvents is spin-coated on top of the

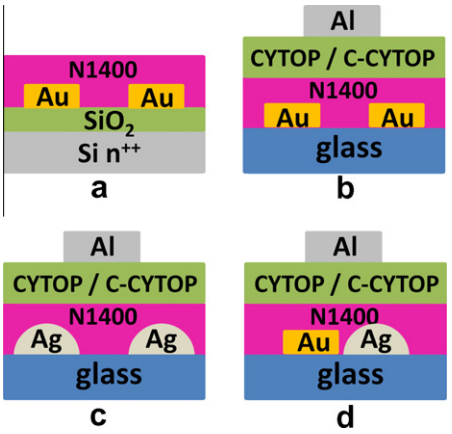

Fig. 1. Schematic illustration of: (a) bottom-gate N1400 FET with lithographically defined bottom Au contacts and SiO_2 dielectric layer; (b) a top-gate FET with lithographically defined bottom Au contacts, a CYTOP based dielectric layer and a top Al gate contact; (c) a top-gate FET with inkjet-printed AgNPs contacts, a CYTOP based dielectric layer and a top Al gate contact; (d) a top-gate FET with asymmetric bottom contacts, one of Au made by photolithography and one of Ag made by inkjet printing.

patterned substrates (~70 nm thick, 1500 rpm, 8 s) in a nitrogen glovebox and then annealed (110 °C, 4 h) to achieve high molecular ordering. The top-gate device is completed by depositing a suitable gate dielectric (450 nm thick Cytop or 50 nm thick Crosslinked Cytop) on top and then by evaporating a thin aluminium gate. All electrical characteristics of the devices were acquired in a nitrogen glovebox or in air with an HP 4155B semiconductor parameter analyzer. The surface morphology of the films was obtained with a Veeco Dimension 3100 (Digital Instruments) atomic force microscope (AFM) operated in the tapping mode. The work-functions (W_f) of printed/evaporated silver contacts were measured by non-contact Scanning Kelvin Probe Microscopy (SKPM) which was carried out in ultrahigh vacuum with an Omicron VT scanning probe microscope. X-ray diffraction (XRD) analysis was performed using a Philips PW1820 X-ray diffractometer in the Bragg-Brentano geometry, with diffraction patterns collected between 2° and 40° with a step size of 0.02° and a dwell time of 2 s per step.

3. Results and discussion

Fig. 2(a) shows the UV-vis optical absorption and photoluminescence (PL) spectra of annealed ActivInk N1400 films spin-coated from chloroform and DCB. For the N1400 films spun from chloroform two main optical absorption peaks located at 525 and 565 nm are observed. When switching the solvent to DCB, the UV-vis spectrum shows a clear red shift of approximately 5 nm for both absorption peaks to 530 nm and 570 nm respectively. Similar red shift is also seen at the emission state of 670 nm in the PL spectrum of N1400 films with DCB as solvent compared to the PL spectrum of N1400 dissolved in chloroform. The red shift in both UV–vis and PL spectra is consistent with a higher degree of thin-film crystallinity [33] obtained when adopting DCB, as confirmed by X-ray diffraction measurements (XRD) reported below. Fig. 2(b) and (c) show the AFM images of

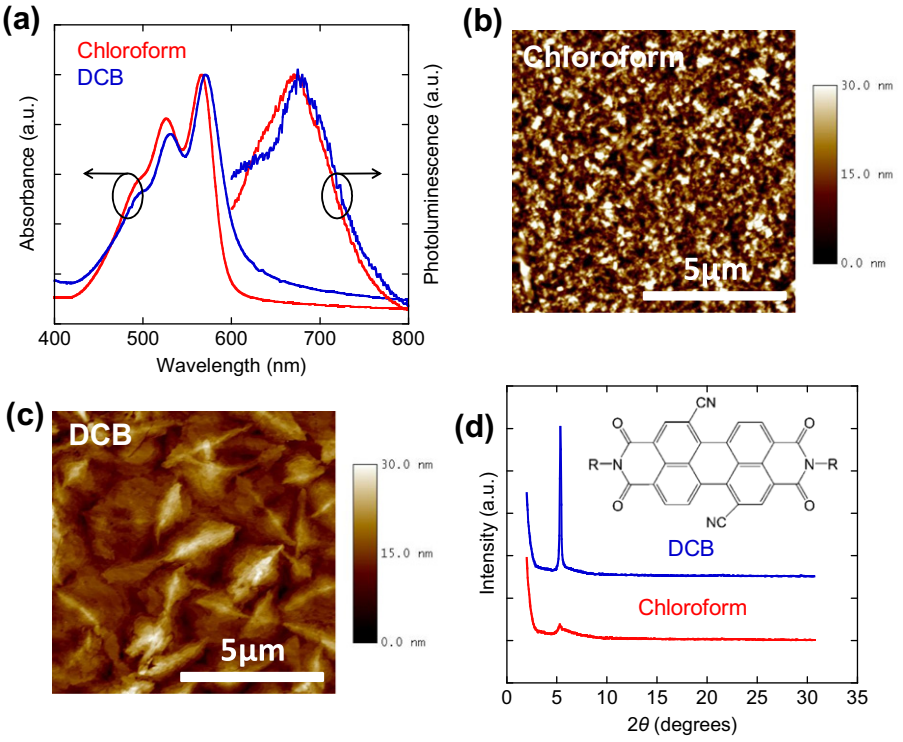

Fig. 2. (a) Normalized UV-Vis absorption and photoluminescence spectra, (b and c) AFM images and (d) X-ray diffraction spectra of corresponding annealed N1400 films spin-coated from chloroform and DCB. The inset of (d) shows the molecular structure of ActivInk N1400.

N1400 films spin-coated from chloroform and DCB, respectively. It is clear that when using chloroform the resulting film consists of very small grains, while with a high boiling point solvent such as DCB, a clear textured microstructure can be induced, probably characterized by a higher degree of molecular order. The roughness of both films, which was previously found to strongly influence the channel mobility [34], are similar, around 3–5 nm. To investigate whether the presence of micron-sized domains in the film spun from DCB is related to formation of micro-crystals, XRD measurements were performed (Fig. 2(d)). The $\theta/2\theta$ scan of N1400 film spun from DCB shows a much pronounced feature at $2\theta = 5.3°$, indicating a significant crystalline thin film microstructure, in contrast to the much weaker reflection peak in the N1400 film from chloroform, suggesting a lower thin film crystallinity.

The electrical characteristics of bottom-gate, bottom-contacts N1400 FETs (Fig. 1(a)) spun from both chloroform and DCB are plotted in Fig. 3(a) and (b). Typical transfer characteristics exhibit a steep current increase in the sub-threshold region; the output characteristics show good saturation behavior for a 20 μm channel. An electron mobility (μ_e) of 0.003 $cm^2\,V^{-1}\,s^{-1}$ is achieved in the saturation region for N1400 processed from chloroform, while μ_e substantially improves to 0.02 $cm^2\,V^{-1}\,s^{-1}$ when DCB is employed. The saturated μ_e is therefore more than one order of magnitude higher for the film spun by DCB compared to the film spun by chloroform and this improvement is mainly attributed to the improved N1400 film crystallinity leading to a much more efficient electron transport in the transistor channel. The increase in the off current for the DCB case also suggests a more favorable bulk charge transport, leading to a higher conductivity even at low charge density. Transfer and output characteristics exhibit negligible hysteresis, meaning that few charge traps are present at the semiconductor/dielectric interface in both cases.

The bottom-contact, top-gate N1400 OFETs (Fig. 1(b)) are further fabricated by using the amorphous fluoropolymer Cytop as the gate dielectric. Fig. 3(c) and (d) summarise the transfer and output characteristics of top-gate, bottom-contact N1400 FET spun from chloroform and DCB. Also in this case the DCB processed devices show strongly improved performances with respect to chloroform processed ones. In the DCB case, the transfer curve demonstrates sharp electron current increase starting from $V_d = -10$ V with small gate leakage currents. μ_e as high as 0.1 $cm^2\,V^{-1}\,s^{-1}$ at $V_d = 40$ V for top-gate configuration with a channel length of 20 μm is extracted with a dielectric capacitance of 4.0 $nF\,cm^{-2}$; the threshold voltage is as small as 1 V and the on-off ratio is $\sim 10^3$–10^4. This top-gate N1400 FET is comparable to the one previously reported by Boudinet et al. [34].

We also tested the bias stress stability of the top-gate, bottom-contacts N1400 OFETs, which is relevant for applications (Fig. 4(a)). The N1400 OFETs have shown bias stress effect with less than 5% current loss when measured under continuous bias ($V_d = 5$ V and $V_g = 40$ V) up to 10 h in a nitrogen glovebox. Poor device bias stability, with a loss of 70% of the current, is instead occurring when the device is measured in air. Although more work is needed to clarify

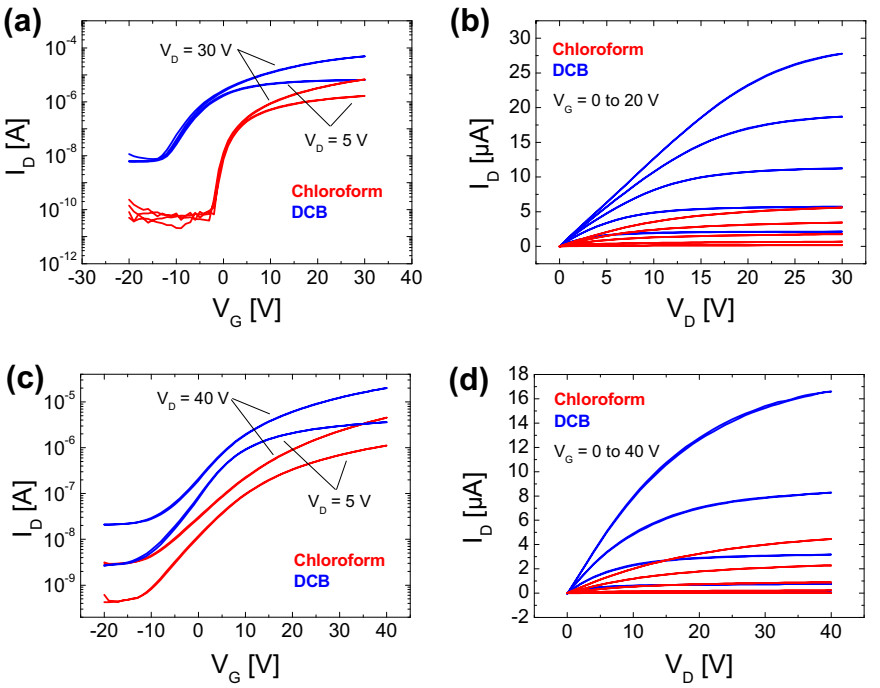

Fig. 3. (a) Transfer and (b) output characteristics, from $V_g = 0$ to $V_g = 20$ V in steps of 5 V, of N1400 OFETs ($L = 20$ μm and $W = 10$ mm) spin-coated from chloroform and DCB in bottom-gate, bottom-contact configuration with SiO_2 (300 nm) as dielectric. (c) Transfer and (d) output characteristics of N1400 OFETs ($L = 20$ μm and $W = 1$ mm) spin-coated from chloroform and DCB in top-gate, bottom-contact configuration with Cytop (450 nm) as dielectric. In all these cases Au contacts were adopted.

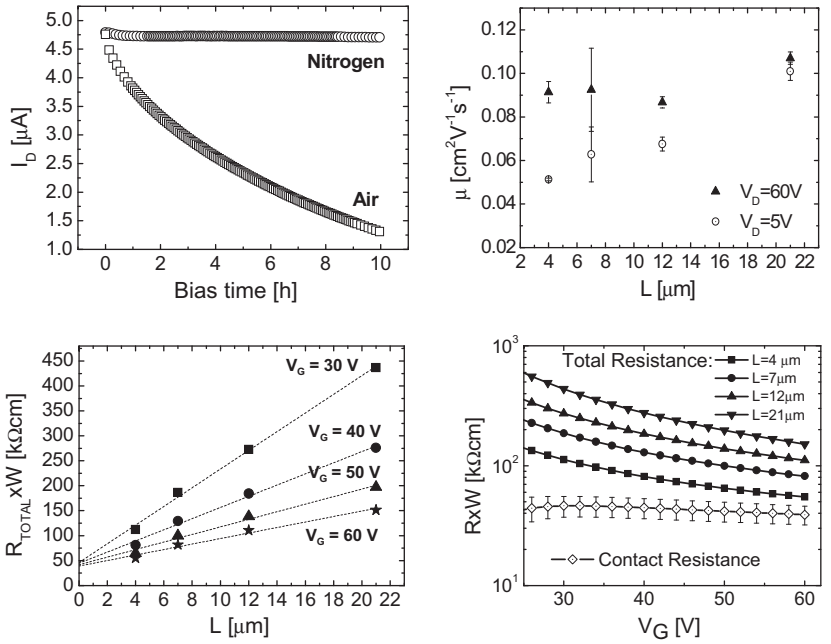

Fig. 4. (a) Bias stress measurements on N1400 top-gate FET ($L = 20$ μm and $W = 1$ mm) in nitrogen (circles) and in air (squares) at $V_d = 5$ V and $V_g = 40$ V. (b) Linear (circles) and saturated (triangles) mobility as a function of the channel length in top-gate N1400 OFETs. (c) Total device resistance in the linear region ($V_d = 5$ V) as a function of the channel length, at different V_g (symbols), for a set of 4 devices with photolithographically defined gold source and drain contacts; the dashed lines indicate the linear extrapolation to zero channel length in order to extract R_C according to TLM. (d) Total resistance (filled symbols) and contact resistance (void symbols) as a function of the gate voltage at $V_d = 5$ V. Data in (b) and (d) are obtained on a set of 16 devices fabricated on the same substrate.

this aspect, the instability in air could be reasonably due to water or oxygen penetration at the semiconductor/dielectric interface despite the presence of the Cytop dielectric which in principle could serve as a barrier layer [35]. To test the device scalability we investigated the contact resistance effect in these *n*-channel OFETs. We adopted a common scaling approach and fabricated N1400 top-gate OFETs with different channel lengths, from 20 to 4 μm. In Fig. 4(b) the linear and saturated mobilities as a function of L are reported. While the saturated mobility is substantially constant in the 0.08–0.11 cm^2/Vs, the linear mobility is apparently decreasing with L as an effect of the contact resistance R_C, passing from 0.10 cm^2/Vs for $L = 21$ μm to 0.05 cm^2/Vs for $L = 4$ μm. In order to estimate R_C we used the well-known transmission line method (TLM, Fig. 4(c)) [36]. Fig. 4(d) shows the plot of the measured total channel resistance and the extracted contact resistance as a function of the gate voltage at $V_d = 5$ V. We have observed a characteristic drop of the total resistance with increasing gate voltage, which is a main characteristic of current crowding effect in staggered device configurations and has been discussed in our previous study [37]. At $V_g = 60$ V we extracted a contact resistance R_C value of 39.1 ± 5.5 kΩcm, consistent with previous experimental results [32]. The measured R_C value is relatively low for electron injection from a high work function electrode in *n*-channel OFETs [23], indicating that N1400 is potentially suitable for downscaled *n*-channel OFETs.

Downscaled, inkjet-printed sub-micrometer OFETs were fabricated in a top-gate, bottom-contact configuration (Fig. 1(c)). For these short channel devices the previously reported self-aligned printing (SAP) technique is adopted [21,38]. However, here we use for the first time printed Ag as the electron injection contact. 1H, 1H, 2H, 2H-perfluorodecanethiol is deposited on photolithographically patterned gold contacts by a vapor process to lower their surface energy. Following this procedure, commercially available AgNPs ink (Harima Chemicals NPS-J, diluted with xylene) is printed within the gap between two confining Au contacts. Due to a limited capability of dewetting showed by the AgNPs ink with respect to our previously adopted Au ink [38], we found that in order to obtain a reliable formation of the SAP channel, the overlap between the AgNPs ink and the Au pattern has to be reduced to a minimum. The AgNPs droplets were consequently printed much closer to one of the two Au contacts, the bottom one in Fig. 5. This, while strongly reducing the process yield on this side because of a not complete dewetting, allows the AgNPs contact line to reliably self-align with the edge of the top gold contact, either because of a dewetting from a very limited overlap or because of the natural expansion of the droplets entirely landed on the glass towards the hydrophobic gold surface. In this case we found that ~80% of the top SAP channels are formed successfully. In the downscaled transistors adopting such electrodes, contacts with printed AgNPs serve as the source to favour electron injection and the patterned gold electrodes serve as the drain. Fig. 5(a) and (b) shows optical images of SAP AgNPs between two patterned gold contacts with SAP channels before and after annealing. As a reference we fabricated also long channel devices (40–60 μm) by printing the same AgNPs ink on glass substrates. In these devices AgNPs function as both source and drain contacts. In either cases, the printed AgNPs are sintered at 220 °C in a nitrogen glovebox for 1 h, turning the AgNPs into a homogeneous metallic contact (~100 nm thick) with shiny, metallic appearance and high electrical conductivity (~10^5 S cm^{-1}). We found that during annealing in air the surface of AgNPs becomes very rough with a large root mean square (rms) roughness of around 60 nm, while AgNP lines annealed under nitrogen exhibit a relatively smooth surface morphology with dramatically reduced rms surface roughness of 9.8 nm (Fig. 5(c)). An AFM image of a SAP sub-micrometer channel is shown in Fig. 5(d). Due to dewetting, the deposited AgNPs ink has been repelled from the surface-modified gold contacts and the average channel length L between gold and printed AgNPs is ~200 nm.

First the electrical characteristics of a long channel N1400 transistor were tested with two printed AgNPs contacts (Fig. 6(a) and (b)). The calculated electron mobility is ~0.07–0.1 $cm^2 V^{-1} s^{-1}$ with a threshold voltage $V_{th} = -1$ V. The mobility is similar to that extracted from standard long channel, top-gate N1400 transistors with photolithographically patterned gold contacts. We find that the sub-micrometer devices ($L = 200$ nm) with AgNPs as source contact and a thick Cytop dielectric (thickness $d = 450$ nm) exhibit typical short channel effects with superlinear increase of drain current and lack of current saturation in the output characteristics. Previous studies on the scaling behaviour for short channel printed transistors showed that when $d/L > 1$ (~1.75 in this case), the transistor exhibits severely degraded characteristics with pronounced short channel effects due to the insufficient downscaling of the gate dielectric [25]. Several methods to decrease the dielectric thickness d for OFETs have been reported, including the use of high-κ metal oxides, self-assembled monolayers (SAMs) or thermally crosslinked polymers [39–41]. In a top-gate configuration the latter approach is the most suitable, although it is challenging to obtain good-quality thin polymer gate dielectrics, principally because thermally-induced crosslinking typically occurs at temperatures incompatible with the underlying organic semiconductor layer and the intrinsic roughness of the organic semiconductor can lead to unacceptable gate leakage. Here we adopt a recently developed crosslinked polymer gate dielectric system fabricated by crosslinking the fluoropolymer dielectric Cytop with 1,6-bis(trichlorosilyl)hexane (C_6-Si) [C-Cytop, inset of Fig. 6(c)] [42]. This approach enables substantial dielectric thickness reduction (down to 50 nm) while retaining high dielectric breakdown strength and small gate leakage current. By adopting a 50 nm thick C-Cytop dielectric, it is possible to fabricate downscaled top-gate N1400 sub-micrometer transistors with AgNPs as source contact exhibiting correctly downscaled transfer and output characteristics (Fig. 6(c) and 6(d)). Thanks to the combination of sub-micrometer channel with a ultrathin gate dielectric, the downscaled N1400 FETs can operate at V_d and $V_g < 5$ V and show a V_{th} of only −0.7 V. The apparent electron mobility of these downscaled FETs is ~2–3 × 10^{-3} $cm^2 V^{-1} s^{-1}$, and the reduction with respect to micron-channel transistors can be mainly attributed to an effect of contact resistances. Accordingly we find that long-channel devices

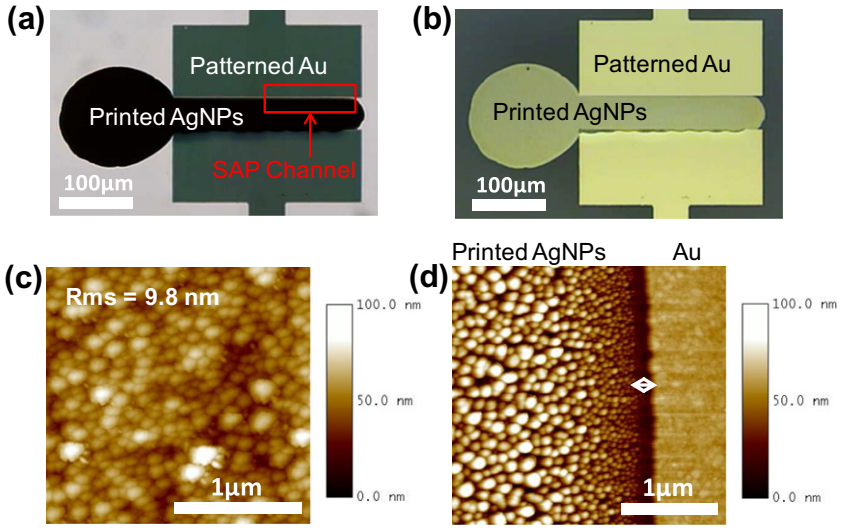

Fig. 5. Optical images of printed AgNPs ink confined between two patterned gold contacts before (a) and after annealing at 220 °C for 1 h (b). (c) AFM image of surface morphology of printed AgNPs annealed in nitrogen and (d) AFM image of the 200 nm channel between printed AgNPs and patterned gold contact.

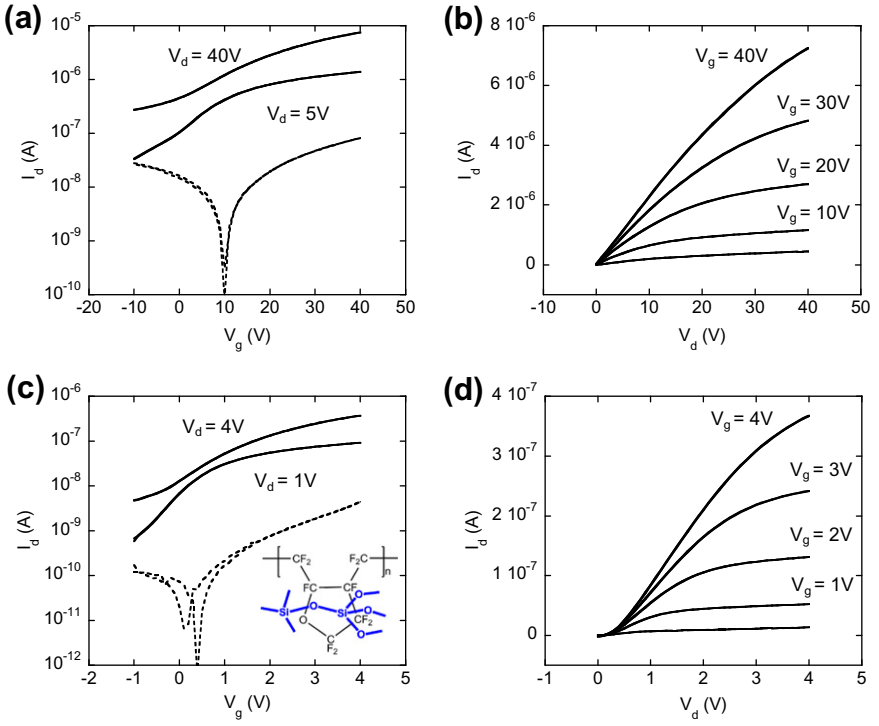

Fig. 6. (a) Transfer and (b) output characteristics of inkjet-printed long channel N1400 OFET with source and drain AgNPs contacts ($L \approx 40$ μm and $W \approx 600$ μm) and Cytop (450 nm) gate dielectric. (c) Transfer and (d) output characteristics of fully downscaled sub-micrometer N1400 FET ($L \approx 200$ nm and $W \approx 300$ μm) using AgNPs as source and ultrathin crosslinked Cytop (C-Cytop, 50 nm) as gate dielectric. The inset of 2(c) indicates the chemical structure of C-Cytop. The gate leakage current is plotted in dashed lines at $V_d = 5$ V and 1 V, respectively.

with C-Cytop exhibit mobilities on the order of 0.07–0.08 $cm^2 V^{-1} s^{-1}$, which are only slightly lower than those of devices with uncrosslinked Cytop (0.07–0.1 $cm^2 V^{-1} s^{-1}$). Therefore the cross-linked, ultrathin dielectric is marginally influencing the overall mobility, likely due to the creation of traps for the electrons. The dominant cause of the mobility degradation in the downscaled device is a contact resistance effect that becomes more critical in such short channels (see discussion below) [25]. Nevertheless, despite of a short channel length ($L = 200$ nm), good drain current saturation is observed in the output characteristics of these FETs, where $d/L \sim 0.25$. To the best of our knowledge this is the

first report of a downscaled *n*-channel organic transistor with inkjet-printed contacts. It is interesting to discuss the impact that the downscaling of the channel length would have on the transition frequency f_T, the maximum operative frequency of the device [43]. In an ideally downscaled device, where the overlap parasitic capacitance is negligible, f_T scales with μL^{-2} [20]. Therefore despite the lower mobility, the 200 nm channel device would show an f_T about 300 times higher than in a 20 μm channel OFET, allowing the device to operate in the MHz regime. This would be enabled by a minimization of the overlap capacitance, for example by implementing the self-aligned gate process, which was demonstrated to be compatible with the present architecture [21].

The normalized drain current ($I_d \times L$) of the downscaled device (L = 200 nm) is significantly lower (by about a factor of 50) than the corresponding current of a long-channel device (L = 60 μm) (Fig. 7(a)), when both transistors are fabricated with the same 50 nm C-Cytop gate dielectric. In other words, instead of inversely scaling with L, the absolute current of the downscaled device is only by a factor of six higher than that of the long channel device. The downscaled device also exhibits less pronounced current saturation and nonlinearity in the output characteristics at small V_d. This deviation from the ideal $1/L$ scaling relationship is a clear manifestation of contact resistance limiting the current in the downscaled devices [17]. If the contact resistance is comparable or exceeds the channel resistance, the apparent carrier mobility drops rapidly with channel length shortening. However, despite of the significant residual contact resistance, the printed silver contacts provide improved electron injection than printed gold contacts. In downscaled devices with two gold contacts we observed very poor transistor operation. This is not surprising since the extrapolated total device resistance from Fig. 4(c), for a 200 nm channel device, results in a value very close to R_C, thus meaning that the lateral voltage would drop mainly on the contacts. This can also be seen by investigating the effect of exchanging the source-drain contacts between printed AgNPs contact and photolithographically patterned gold contact in our asymmetric sub-micrometer channels. The corresponding transfer characteristics are shown in Fig. 7(b), indicating a substantial difference of drain currents by switching the contacts. For the same device, the measured drain current is much higher when using the printed AgNPs as source than when using the gold electrode as source. Both linear and saturated currents obtained with AgNPs biased as source are one order of magnitude larger than those obtained with gold biased as source. We believe that this improvement is the result of the lower electron injection barrier of AgNPs vs. Au. In fact it was previously reported that, with respect to devices employing bare Au electrodes, a lower contact resistance for N1400 TC FETs can be achieved by a better matching of the contact W_f with the LUMO level of N1400 (4.3 eV), thanks to surface modification of the contacts [32]. We therefore employed Scanning Kelvin Probe Microscopy (SKPM) to measure

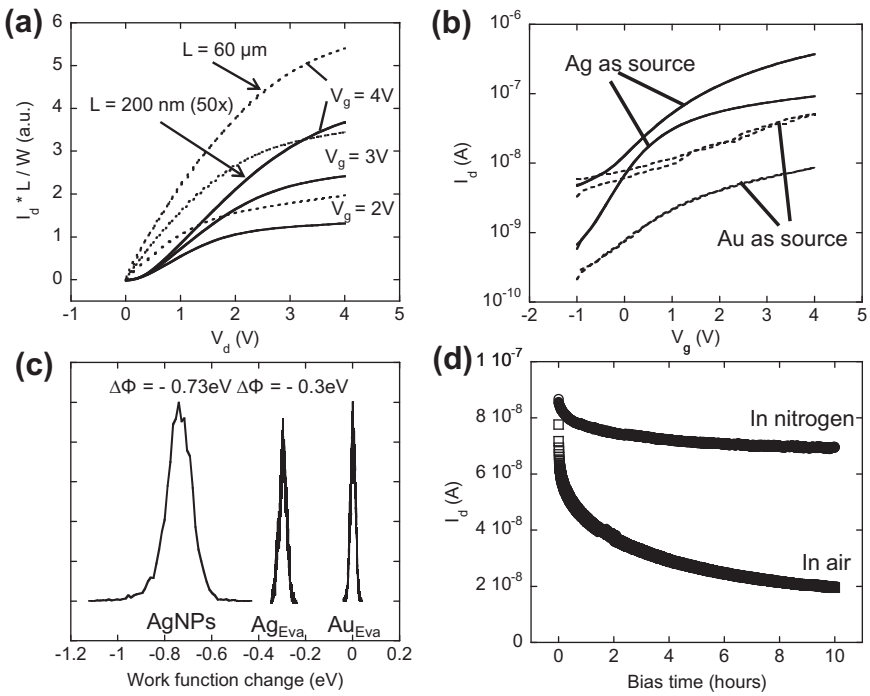

Fig. 7. (a) Scaling of output characteristics of N1400 transistors normalized by multiplying the drain current by the channel length and by dividing by the channel width (dashed line, $L \approx 60$ μm, $W \approx 600$ μm with printed Ag-Ag contacts; solid line, $L \approx 200$ nm, $W \approx 300$ μm with SAP Ag-Au contacts). The scaled output current ($I_d \times L$) of the SAP device is multiplied by a factor of 50. (b) Transfer characteristics of the 200 nm channel FET by switching source/drain contacts between AgNPs and gold. (c) Histogram of work-function changes ($\Delta\Phi$) with respect to evaporated gold (Au_{Eva}), evaporated silver (Ag_{Eva}) and printed AgNPs measured by SKPM. (d) Bias stress on downscaled N1400 FET at V_d = 1 V and V_g = 4 V measured in nitrogen and in air.

the work-function differences ($\Delta\Phi$) for the electrodes adopted in the present work. Fig. 7(c) shows the measured $\Delta\Phi$ for printed AgNPs and evaporated gold (Au_{Eva}); we also characterized evaporated silver (Ag_{Eva}) for comparison. We found that Ag_{Eva} work-function is lower by 0.3 eV than that of Au_{Eva}, but the printed AgNPs surface work-function is 0.73 eV lower than that of evaporated gold. The fact that the printed AgNPs W_f is lower than that of Ag_{Eva} after air exposure might be the result of residual organic ligands present on the AgNPs surface after annealing, or could be a manifestation of an improved air stability of printed AgNPs films compared to evaporated silver films. However, the SKPM results are fully consistent with the printed AgNPs contacts providing a better electron injection into the organic semiconductor than Au. This is because the OFET performance is expected to be more sensitive to the contact resistance present at the reverse biased source contact than at the forward biased drain contact [23,37].

Finally, we have also investigated the bias stress of the N1400 downscaled FETs both in a nitrogen glovebox and in air (Fig. 7(d)). While applying a continuous bias to the transistor (V_d = 1 V and V_g = 4 V) for 10 hours, we measured the drain current of the device. In the nitrogen glovebox the current decreased by ~20%, while in the device that underwent bias stress in air exhibited a more serious current decay, which reached 75% of the initial current after 10 h. As in the previous case, this is probably due to the penetration of oxygen and/or water through the ultra-thin dielectric film into the device channel region. These stress data are significantly better than those previously obtained with micron-channel F8T2 *p*-channel transistors with C-Cytop operated under the same conditions [42]. Furthermore, they are consistent with the bias stress result on N1400 micron-channel transistors with C-Cytop, where a 35% and 74% reduction in electron current were obtained under nitrogen and in air, respectively. These results confirm that the printed sub-micrometer channel architecture does not substantially influence the device stability under bias stress conditions.

4. Conclusion

In summary, we reported the successful downscaling of *n*-channel FETs with inkjet-printed source-drain electrodes and N1400 as the semiconductor. Electron mobilities >0.1 $cm^2 V^{-1} s^{-1}$ can be obtained in long channel devices with a high boiling point solvent thanks to the formation of highly textured semiconductor films. Crisp current saturation for operating voltages lower than 5 V was achieved for a 200 nm channel length when using inkjet printed AgNPs as source electrode and a 50 nm thick C-Cytop film as gate dielectric. The sub-micrometer inkjet printed AgNPs contacts do not affect the device bias stability and show improved electron injection, with smaller contact resistance, compared to Au contacts. Given the demonstrated compatibility of N1400 with polymeric substrates [32] and the availability of metallic inks with low sintering temperatures (<150 °C) [38], also compatible with the gate contact patterning, it should be possible on the basis of the present demonstration, to develop downscaled *n*-channel OFET devices compatible with low-cost, large area manufacturing of flexible electronics, provided a suitable coating technique, alternative to spin-coating, is developed for the active and dielectric layers [44–46]. While further reduction of the contact resistance is still required, downscaled, printed *n*-channel N1400 transistors could therefore provide an important building block for the fabrication of printed organic complementary circuits.

Acknowledgments

The authors would like to thank Dr. Ni Zhao, Dr. Enrico Gili, Dr. Jui-fen Chang, Dr. S. Lu, Dr. Z. Chen and Feng Gao for experimental support. Polyera Corporation acknowledges the Flextech Allience for the support of ActivInk development. This work was supported by the EU Integrated Project NAIMO (NMP4-CT-2004-500355).

References

[1] (a) Facchetti A, Π-conjugated polymers for organic electronics and photovoltaic cell applications, Chem. Mater. 23 (2011) 733–758; (b) D. Boudinet, M. Benwadih, S. Altazin, J. Verilhac, E. De Vito, C. Serbutoviez, G. Horowitz, A. Facchetti, Influence of the substrate surface chemistry on the performance of top-gate organic thin-film transistors, J. Am. Chem. Soc. 133 (2011) 9968–9971.
[2] I. McCulloch, M. Heeney, C. Bailey, K. Genevicius, I. Macdonald, M. Shkunov, D. Sparrowe, S. Tierney, R. Wagner, W.M. Zhang, M.L. Chabinyc, R.J. Kline, M.D. McGehee, M.F. Toney, Liquid-crystalline semiconducting polymers with high charge-carrier mobility, Nat. Mater. 5 (2006) 328–333.
[3] R.S. Ashraf, Z. Chen, D.S. Leem, H. Bronstein, W. Zhang, B. Schroeder, Y. Geerts, J. Smith, S. Watkins, T.D. Anthopoulos, H. Sirringhaus, J.C. de Mello, M. Heeney, I. McCulloch, Silaindacenodithiophene semiconducting polymers for efficient solar cells and high-mobility ambipolar Transistorsâ€, Chem. Mater. 23 (2011) 768–770.
[4] G. Gelinck, P. Heremans, K. Nomoto, T.D. Anthopoulos, Organic transistors in optical displays and microelectronic applications, Adv. Mater. 22 (2010) 3778–3798.
[5] H. Klauk, Organic thin-film transistors, Chem. Soc. Rev. 39 (2010) 2643–2666.
[6] H. Klauk, U. Zschieschang, J. Pflaum, M. Halik, Ultralow-power organic complementary circuits, Nature 445 (2007) 745–748.
[7] H. Minemawari, T. Yamada, H. Matsui, J.y. Tsutsumi, S. Haas, R. Chiba, R. Kumai, T. Hasegawa, Inkjet printing of single-crystal films, Nature 475 (2011) 364–367.
[8] Y. Zhao, C.-a. Di, X. Gao, Y. Hu, Y. Guo, L. Zhang, Y. Liu, J. Wang, W. Hu, D. Zhu, All-solution-processed, high-performance n-channel organic transistors and circuits: toward low-cost ambient electronics, Adv. Mater. 23 (2011) 2448–2453.
[9] H. Sirringhaus, P.J. Brown, R.H. Friend, M.M. Nielsen, K. Bechgaard, B.M.W. Langeveld-Voss, A.J.H. Spiering, R.A.J. Janssen, E.W. Meijer, P. Herwig, D.M. de Leeuw, Two-dimensional charge transport in self-organized, high-mobility conjugated polymers, Nature 401 (1999) 685–688.
[10] H. Yan, Z.H. Chen, Y. Zheng, C. Newman, J.R. Quinn, F. Dotz, M. Kastler, A. Facchetti, A high-mobility electron-transporting polymer for printed transistors, Nature 457 (2009) 679–686.
[11] M. Caironi, M. Bird, D. Fazzi, Z. Chen, R. Di Pietro, C. Newman, A. Facchetti, H. Sirringhaus, very low degree of energetic disorder as the origin of high mobility in an n-channel polymer semiconductor, Adv. Funct. Mater. 21 (2011) 3371–3381.
[12] A.C. Arias, S.E. Ready, R. Lujan, W.S. Wong, K.E. Paul, A. Salleo, M.L. Chabinyc, R. Apte, R.A. Street, Y. Wu, P. Liu, B. Ong, All jet-printed polymer thin-film transistor active-matrix backplanes, Appl. Phys. Lett. 85 (2004) 3304–3306.
[13] K.J. Lee, M.J. Motala, M.A. Meitl, W.R. Childs, E. Menard, A.K. Shim, J.A. Rogers, R.G. Nuzzo, Large-area, selective transfer of microstructured silicon: a printing-based approach to high-performance thin-film transistors supported on flexible substrates, Adv. Mater. 17 (2005) 2332–2336.
[14] J.U. Park, M. Hardy, S.J. Kang, K. Barton, K. Adair, D.K. Mukhopadhyay, C.Y. Lee, M.S. Strano, A.G. Alleyne, J.G. Georgiadis, P.M. Ferreira, J.A.

Rogers, High-resolution electrohydrodynamic jet printing, Nat. Mater. 6 (2007) 782–789.
[15] (15a) K.-J. Baeg, D. Khim, D.-Y. Kim, S.-W. Jung, J.B. Koo, I.-K. You, H. Yan, A. Facchetti, Y.-Y. Noh, High speeds complementary integrated circuits fabricated with all-printed polymeric semiconductors, J. Polym. Sci., Part B: Polym. Phys. 49 (2011) 62–67;
(15b) K.-J. Baeg, D.-Y. Kim, D. Khim, M. Caironi, Dong-Yu, I-K. You, J. Quinn, A. Facchetti, Y.-Y. Noh, Charge Injection engineering of ambipolar field-effect transistors for high performance organic complementary circuits, ACS Appl. Mater. Interfaces 3 (2011) 3205–3214.
[16] X. Li, W.T.T. Smaal, C. Kjellander, B. van der Putten, K. Gualandris, E.C.P. Smits, J. Anthony, D.J. Broer, P.W.M. Blom, J. Genoe, G. Gelinck, Charge transport in high-performance ink-jet printed single-droplet organic transistors based on a silylethynyl substituted pentacene/insulating polymer blend, Org. Electron. 12 (2011) 1319–1327.
[17] H. Sirringhaus, T. Kawase, R.H. Friend, T. Shimoda, M. Inbasekaran, W. Wu, E.P. Woo, High-resolution inkjet printing of all-polymer transistor circuits, Science 290 (2000) 2123–2126.
[18] C.W. Sele, T. von Werne, R.H. Friend, H. Sirringhaus, Lithography-free, self-aligned inkjet printing with sub-hundred-nanometer resolution, Adv. Mater. 17 (2005) 997–1001.
[19] T. Sekitani, Y. Noguchi, U. Zschieschang, H. Klauk, T. Someya, Organic transistors manufactured using inkjet technology with subfemtoliter accuracy, Proc. Natl Acad. Sci. USA 105 (2008) 4976–4980.
[20] M. Caironi et al., solution-processed organic field-effect transistors, Semicond. Sci. Technol. 26 (2011) 034006.
[21] Y.-Y. Noh, N. Zhao, M. Caironi, H. Sirringhaus, Downscaling of self-aligned, all-printed polymer thin-film transistors, Nat. Nano 2 (2007) 784–789.
[22] S.P. Tiwari, X.H. Zhang, W.J. Potscavage, B. Kippelen, Study of electrical performance and stability of solution-processed n-channel organic field-effect transistors, J. Appl. Phys. 106 (2009) 6.
[23] M. Caironi, C. Newman, J.R. Moore, D. Natali, H. Yan, A. Facchetti, H. Sirringhaus, Efficient charge injection from a high work function metal in high mobility n-type polymer field-effect transistors, Appl. Phys. Lett. 96 (2010) 183303.
[24] T.H. Jung, B. Yoo, L. Wang, A. Dodabalapur, B.A. Jones, A. Facchetti, M.R. Wasielewski, T.J. Marks, Nanoscale n-channel and ambipolar organic field-effect transistors, Appl. Phys. Lett. 88 (2006) 3.
[25] Y.Y. Noh, N. Zhao, M. Caironi, H. Sirringhaus, Downscaling of self-aligned, all-printed polymer thin-film transistors, Nat. Nanotechnol. 2 (2007) 784–789.
[26] N. Zhao, M. Chiesa, H. Sirringhaus, Y.N. Li, Y.L. Wu, Self-aligned inkjet printing of highly conducting gold electrodes with submicron resolution, J. Appl. Phys. 101 (2007) 6.
[27] H. Yan, Y. Zheng, R. Blache, C. Newman, S.F. Lu, J. Woerle, A. Facchetti, Solution processed top-gate n-channel transistors and complementary circuits on plastics operating in ambient conditions, Adv. Mater. 20 (2008) 3393–3398.
[28] B.A. Jones, M.J. Ahrens, M.H. Yoon, A. Facchetti, T.J. Marks, M.R. Wasielewski, High-mobility air-stable n-type semiconductors with processing versatility: Dicyanoperylene-3,4: 9,10-bis(dicarboximides), Angew. Chem.-Int. Edit. 43 (2004) 6363–6366.
[29] A.S. Molinari, H. Alves, Z. Chen, A. Facchetti, A.F. Morpurgo, High electron mobility in vacuum and ambient for PDIF-CN2 single-crystal transistors, J. Am. Chem. Soc. 131 (2009) 2462–2463.
[30] C. Piliego, D. Jarzab, G. Gigli, Z.H. Chen, A. Facchetti, M.A. Loi, High electron mobility and ambient stability in solution-processed perylene-based organic field-effect transistors, Adv. Mater. 21 (2009) 1573–1576.
[31] T.N. Ng, S. Sambandan, R. Lujan, A.C. Arias, C.R. Newman, H. Yan, A. Facchetti, Electrical stability of inkjet-patterned organic complementary inverters measured in ambient conditions, Appl. Phys. Lett. 94 (2009) 3.
[32] D. Boudinet, M. Benwadih, Y.B. Qi, S. Altazin, J.M. Verilhac, M. Kroger, C. Serbutoviez, R. Gwoziecki, R. Coppard, G. Le Blevennec, A. Kahn, G. Horowitz, Modification of gold source and drain electrodes by self-assembled monolayer in staggered n- and p-channel organic thin film transistors, Org. Electron. 11 (2010) 227–237.
[33] J. Clark, C. Silva, R.H. Friend, F.C. Spano, Role of intermolecular coupling in the photophysics of disordered organic semiconductors: aggregate emission in regio regular polythiophene, Phys. Rev. Lett. 98 (2007) 4.
[34] D. Boudinet, M. Benwadih, S. Altazin, R. Gwoziecki, J.M. Verilhac, R. Coppard, G. Le Blevennec, I. Chartier, G. Horowitz, Influence of the semi-conductor layer thickness on electrical performance of staggered n- and p-channel organic thin-film transistors, Org. Electron. 11 (2010) 291–298.
[35] J. Granstrom, J.S. Swensen, J.S. Moon, G. Rowell, J. Yuen, A.J. Heeger, Encapsulation of organic light-emitting devices using a perfluorinated polymer, Appl. Phys. Lett. 93 (2008) 3.
[36] J. Zaumseil, K.W. Baldwin, J.A. Rogers, Contact resistance in organic transistors that use source and drain electrodes formed by soft contact lamination, J. Appl. Phys. 93 (2003) 6117–6124.
[37] T. Richards, M. Bird, H. Sirringhaus, A quantitative analytical model for static dipolar disorder broadening of the density of states at organic heterointerfaces, J. Chem. Phys. 128 (2008) 234905.
[38] M. Caironi, E. Gili, T. Sakanoue, X. Cheng, H. Sirringhaus, High yield, single droplet electrode arrays for nanoscale printed electronics, ACS Nano 4 (2010) 1451–1456.
[39] M. Halik, H. Klauk, U. Zschieschang, G. Schmid, C. Dehm, M. Schutz, S. Maisch, F. Effenberger, M. Brunnbauer, F. Stellacci, Low-voltage organic transistors with an amorphous molecular gate dielectric, Nature 431 (2004) 963–966.
[40] L.L. Chua, P.K.H. Ho, H. Sirringhaus, R.H. Friend, High-stability ultrathin spin-on benzocyclobutene gate dielectric for polymer field-effect transistors, Appl. Phys. Lett. 84 (2004) 3400–3402.
[41] M.H. Yoon, H. Yan, A. Facchetti, T.J. Marks, Low-voltage organic field-effect transistors and inverters enabled by ultrathin cross-linked polymers as gate dielectrics, J. Am. Chem. Soc. 127 (2005) 10388–10395.
[42] X. Cheng, M. Caironi, Y.-Y. Noh, J. Wang, C. Newman, H. Yan, A. Facchetti, H. Sirringhaus, Air stable cross-linked cytop ultrathin gate dielectric for high yield low-voltage top-gate organic field-effect transistors, Chem. Mater. 22 (2010) 1559–1566.
[43] V. Wagner, P. Wöbkenberg, A. Hoppe, J. Seekamp, Megahertz operation of organic field-effect transistors based on poly(3-hexylthiopene), Appl. Phys. Lett. 89 (2006) 243515.
[44] J.-M. Verilhac, M. Benwadih, A.-L. Seiler, S. Jacob, C. Bory, J. Bablet, M. Heitzman, J. Tallal, L. Barbut, P. Frère, G. Sicard, R. Gwoziecki, I. Chartier, R. Coppard, C. Serbutoviez, Step toward robust and reliable amorphous polymer field-effect transistors and logic functions made by the use of roll to roll compatible printing processes, Org. Electron. 11 (2010) 456–462.
[45] M. Hambsch, K. Reuter, M. Stanel, G. Schmidt, H. Kempa, U. Fügmann, U. Hahn, A.C. Hübler, Uniformity of fully gravure printed organic field-effect transistors, Mater. Sci. Eng., B 170 (2010) 93–98.
[46] M.M. Voigt, A. Guite, D.-Y. Chung, R.U.A. Khan, A.J. Campbell, D.D.C. Bradley, F. Meng, J.H.G. Steinke, S. Tierney, I. McCulloch, H. Penxten, L. Lutsen, O. Douheret, J. Manca, U. Brokmann, K. Sönnichsen, D. Hülsenberg, W. Bock, C. Barron, N. Blanckaert, S. Springer, J. Grupp, A. Mosley, Polymer field-effect transistors fabricated by the sequential gravure printing of polythiophene, two insulator layers, and a metal ink gate, Adv. Funct. Mater. 20 (2010) 239–246.